Geodesic Lower Bound of the Energy Consumption to Achieve Membrane Separation within Finite Time

Jin-Fu Chen,[1,2,3] Ruo-Xun Zhai,[2] C. P. Sun,[1,2] and Hui Dong[2,*]

[1] *Beijing Computational Science Research Center, 100193 Beijing, China*

[2] *Graduate School of China Academy of Engineering Physics, No. 10 Xibeiwang East Road, Haidian District, 100193 Beijing, China*

[3] *Present address: School of Physics, Peking University, 100871 Beijing, China*

(Received 25 October 2022; revised 20 May 2023; accepted 6 June 2023; published 19 July 2023)

With its promise for low energy consumption, membrane technology has stimulated efficient approaches to separate mixtures. Technological progress has been made to achieve better purification with lower energy cost and higher productivity. Separation with high productivity is typically accomplished within a limited operation time, which unavoidably results in an excess energy consumption due to the fundamental laws of thermodynamics. Reduction of the energy consumption is of practical importance in the application of membrane separation. However, little is known about the fundamental limit of the least excess energy consumption in a finite operation time. We derive such a limit for the separation of binary mixed gases and show its proportionality to the square of the geometric distance between the initial state and the final state and its inverse proportionality to the operation time. The result shows that optimizing the separation protocol is equivalent to finding the geodesic curve in a geometric space. We predict that for the symmetric protocols, the complete separation of 1 mol of a binary mixture of equally mixed ideal single-atom gases at environmental temperature T_0 within operation time τ requires at least $(12-8\sqrt{2})N_A k_B T_0 \tau_p/\tau$ for a particle-transport-dominated process and $2(\ln 2)^2 N_A k_B T_0 \tau_h/3\tau$ for a heat-exchange-dominated process, where N_A is the Avogadro number and τ_p and τ_h are the timescales for particle transport and heat exchange, respectively. Interestingly, for a symmetric system, the minimum excess energy consumption is achieved by symmetry-breaking protocols. Our geometric approach may inspire the optimization of industrial membrane separation protocols.

DOI: 10.1103/PRXEnergy.2.033003

I. INTRODUCTION

Separating components in a mixture into a purer form is of crucial importance in various industrial applications [1,2], e.g., in water purification [3,4], tail gas purification [1], and pharmaceutical production [5–7]. Traditional methods of separation such as distillation or chemical purification usually have a large energy and environmental cost. In water purification, distilling 1 m^3 of seawater has an energy cost of about 640 kW h. With clever optimization of heat transfer and process design, such cost can be reduced to around 50 kW h [8,9]. The flourishing of membrane science and technology in recent decades has provided a more efficient approach to achieve separation of components [10–14], with a significant reduction of the energy cost to roughly 4.5 kW h [8,15] and a considerable increase in energy efficiency. Since the 1960s, there have been three generations of membrane separation technology, represented by the ultrafiltration or microfiltration membrane system, the aqueous reverse osmosis system, and refined size discrimination [16], with the use extended from water purification [17,18] to the separation of gas molecules, such as acquiring N_2 from the air or removing CO_2 from natural gas [19,20]. Such membrane technology has also benefited the pharmaceutical and biological industries [21,22], the environmental science of CO_2 controls [23–25], the food industry [26], and the development of renewable energy resources [27–29].

To increase the performance of membrane separation, significant efforts have been made with existing membrane apparatus from different perspectives, e.g., developing new-generation material with greater selectivity and permeability to the required components [12,19,30,31] to ensure the purity of the product, and designing new separation modules to reduce energy cost and optimize durability

*hdong@gscaep.ac.cn

[32,33]. Productivity, defined as the generation rate for the target product in the separation process, has always been one of the determining factors for whether an industrial separation approach is economically practical [34]. However, there exists a trade-off between productivity and energy consumption in separation processes—increasing productivity to complete the purification within a shorter operation time is usually accompanied by an excess energy consumption [35]. For example, the simulation result in Ref. [33] shows for a CO_2 capture device combining membrane separation and cultivation of algae that the energy consumption increases from 0.5 MJ/kg CO_2 to more than 200 MJ/kg CO_2 when the feed rate increases from 0.01 to 10 kmol/s. Given such considerable excess energy consumption, optimizing such a trade-off relation is important.

Recently, the development of finite-time thermodynamics has spurred a theoretical revisit of the membrane process for better purification. The fundamental laws of the thermodynamics of equilibrium processes define a universal lower limit for arbitrary separation processes $W \geq \Delta F$ [36,37], but actual separation processes are typically accomplished within a finite operation time. Such nonequilibrium processes must be investigated [38–40] to reveal the excess energy consumption beyond the lower limit given by the fundamental laws of thermodynamics of equilibrium processes. An important question that arises naturally is whether there is a lower bound to the energy consumption in finite time posited by the fundamental laws of thermodynamics. If there is, such a bound should allow us to reduce the excess energy consumption of these separation processes without reducing productivity, and should shed light on the material synthesis and the module design of separation processes.

In this work, we seek a fundamental bound of the least energy consumption in a finite operation time as a consequence of the basic law of finite-time thermodynamics. With a geometric structure of the thermal equilibrium configuration space [41–49], we determine that the minimum excess energy consumption is proportional to the square of the distance between the initial state and the final state. For a practical finite-time separation process, the excess energy consumption beyond the quasistatic separation should be optimized to reach the fundamental limit [40,50–52]. By using the revised Fick's law of diffusion [53], we convert such a task of finding the minimum energy consumption in a gas separation process into finding the shortest path in a configuration space, demonstrating the first application of geometric optimization in the membrane separation process.

II. MODELING THE MEMBRANE SEPARATION

Consider a binary mixture of gas molecules in a chamber with volume V_t, as illustrated in Fig. 1(a). The system is immersed in a thermal bath with temperature T_0. The two species of molecules are represented by blue pyramids (type α) and red balls (type β), and the numbers of molecules for each species are denoted by N_α and N_β. The separation process is performed by mechanically moving two semipermeable membranes, A and B, towards each other from opposite ends of the chamber. Membrane A (membrane B) is designed with properties allowing perfectly selective permeability, i.e., allowing only type-α (type-β) molecules to penetrate. The chamber is divided into three compartments with the two membranes: the left one with volume V_L for the purified type-α molecules,

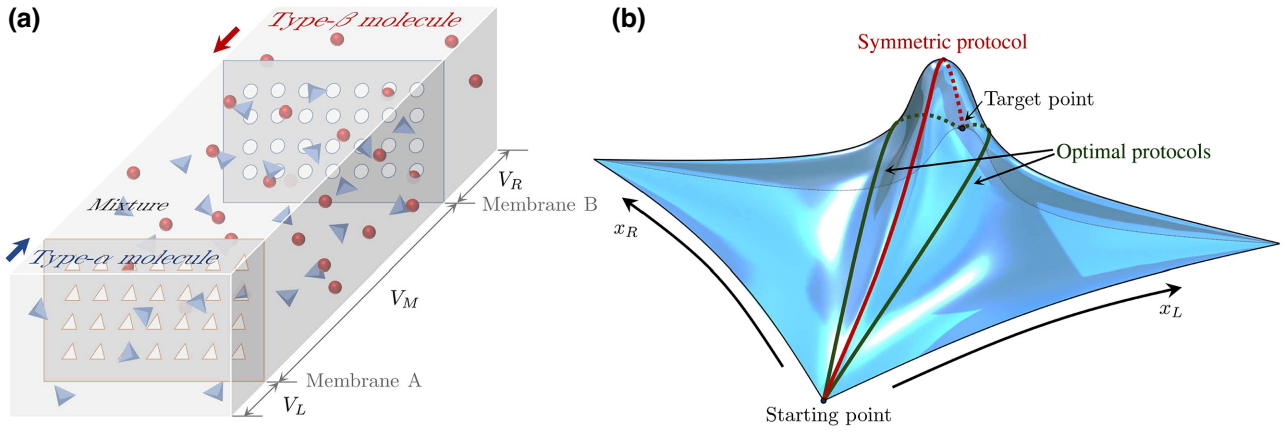

FIG. 1. Separation of two mixed gases. (a) The separation process. The chamber is divided into three compartments, the left one (with volume V_L) for the purified type-α molecules (blue pyramids), the middle one (with volume V_M) for the molecular mixture, and the right one (with volume V_R) for the purified type-β molecules (red balls). Semipermeable membranes A and B are designed to allow only type-α and type-β molecules to pass through them, respectively. During the separation process, the two membranes are pushed towards each other. (b) The landscape of the configuration space spanned by $x^k = V_k/V_t$ $(k = L, R)$ for the separation process. The lengths of the paths between the starting point (0,0) and the target point (0.5,0.5) reflect the excess energy consumption of the corresponding protocols.

the middle one with volume V_M for the molecular mixture, and the right one with volume V_R for the purified type-β molecules. The three volumes satisfy the condition $V_L + V_M + V_R = V_t$. At the end of the separation, membranes A and B contact each other, i.e., $V_M = 0$, and the two gases are purified in the left and right compartments.

We denote the number of type-σ ($\sigma = \alpha, \beta$) molecules in compartment k ($k = L, M, R$) as $N_{\sigma k}$. The impermeability of membrane A (membrane B) to type-β (type-α) molecules results in $N_{\beta L} = N_{\alpha R} = 0$. For gas molecules, the relaxation time is typically far shorter than the operation time. Such a situation is typically referred to as the "endoreversible region" [38,39], where the status of the gas can be described by macroscopic parameters, i.e., the pressure and the temperature. We assume the heat exchange between the compartments is fast enough to establish a global temperature T for the molecules in the whole chamber. The hydrodynamic effects in the transport of the gases are ignored. The states of the gases in each compartment are described by the van der Waals equation

$$p_k + a_k \frac{N_k^2}{V_k^2} = \frac{N_k k_B T}{V_k - N_k b_k}, \tag{1}$$

where p_k is the pressure in each compartment k with particle number $N_k = N_{\alpha k} + N_{\beta k}$, k_B is the Boltzmann constant, and a_k and b_k are the van der Waals constants—a_k is a measure of the interaction strength between molecules and b_k is the volume of a single molecule. In each compartment k, a_k and b_k are related to the mixture ratios $\eta_{\alpha k} = N_{\alpha k}/N_k$ and $\eta_{\beta k} = N_{\beta k}/N_k = 1 - \eta_{\alpha k}$ via the relations $a_k = a_{\alpha\alpha}\eta_{\alpha k}^2 + 2a_{\alpha\beta}\eta_{\alpha k}\eta_{\beta k} + a_{\beta\beta}\eta_{\beta k}^2$ and $b_k = b_{\alpha\alpha}\eta_{\alpha k}^2 + 2b_{\alpha\beta}\eta_{\alpha k}\eta_{\beta k} + b_{\beta\beta}\eta_{\beta k}^2$, where $a_{\sigma\sigma}$ and $b_{\sigma\sigma}$ are the van der Waals constants for pure type-σ gas, $a_{\alpha\beta}$ is related to the interaction between two van der Waals gases, and $b_{\alpha\beta}$ is the impenetrable volume for the collision between α-type and β-type molecules, given by $b_{\alpha\beta} = [(b_{\alpha\alpha}^{1/3} + b_{\beta\beta}^{1/3})/2]^3$.

During quasistatic separation processes, the gases have sufficient time to reach equilibrium with the bath, and the gas temperature is equal to the bath temperature $T = T_0$. However, during finite-time separation processes, the gas temperature T typically deviates from the bath temperature T_0 due to the finite duration of the operation.

Two types of relaxation occur in the separation process: particle transport across the membranes and heat conduction through the wall of the chamber. To describe the relaxation of particle transport, we derive a revised Fick's law of diffusion for van der Waals gases as follows (see the derivation in Appendix A):

$$\begin{aligned}
\dot{N}_{\alpha L} &= \kappa_\alpha \mathcal{A} k_B T \left[(c_{\alpha M} - c_{\alpha L}) \right. \\
&\quad \left. + \left(b - \frac{a}{k_B T} \right) c_{\beta M}(c_{\alpha M} + c_{\alpha L}) \right], \\
\dot{N}_{\beta R} &= \kappa_\beta \mathcal{A} k_B T \left[(c_{\beta M} - c_{\beta R}) \right. \\
&\quad \left. + \left(b - \frac{a}{k_B T} \right) c_{\alpha M}(c_{\beta M} + c_{\beta R}) \right],
\end{aligned} \tag{2}$$

where $c_{\sigma k} = N_{\sigma k}/V_k$ is the density of type-σ molecules in compartment k, κ_α (κ_β) is the diffusion constant of type-α (type-β) molecules across membrane A (membrane B), and $\mathcal{A}$ is the area of the membranes, which is assumed to be the same for membranes A and B. In the derivation, we assume that $a_{\alpha\alpha} = a_{\alpha\beta} = a_{\beta\beta} = a$ and $b_{\alpha\alpha} = b_{\alpha\beta} = b_{\beta\beta} = b$. As a result, the van der Waals constants of the mixed gases are the same as those of pure type-α and type-β gases. The second term on the right-hand side is the correction to Fick's law due to the interaction energy of van der Waals gases. Here we keep the correction terms to the first order of the van der Waals constants.

We use Newton's law of cooling to describe the heat conduction between the system and the thermal bath, i.e., $\dot{Q} = -C_V \gamma (T - T_0)$, where C_V is the heat capacity of the system at constant volume, e.g., $C_V = (3/2)N_t k_B$ for a single-atom ideal gas with total number $N_t = N_\alpha + N_\beta$ of the two types of molecules, and γ is the cooling rate of the system. With the first law of thermodynamics, the evolution of the gas temperature T is governed by the differential equation (see the derivation in Appendix B)

$$\begin{aligned}
\dot{T} &= -\gamma(T - T_0) - \frac{k_B T}{C_V} \left[\frac{N_{\alpha L}\dot{V}_L}{V_L - N_{\alpha L} b} + \frac{\left(N_{\alpha M} + N_{\beta M}\right)\dot{V}_M}{V_M - (N_{\alpha M} + N_{\beta M}) b} + \frac{N_{\beta R}\dot{V}_R}{V_R - N_{\beta R} b} \right] \\
&\quad + \frac{2a\dot{N}_{\alpha L}}{C_V} \left(\frac{N_{\alpha M} + N_{\beta M}}{V_M} - \frac{N_{\alpha L}}{V_L} \right) + \frac{2a\dot{N}_{\beta R}}{C_V} \left(\frac{N_{\alpha M} + N_{\beta M}}{V_M} - \frac{N_{\beta R}}{V_R} \right),
\end{aligned} \tag{3}$$

where the first term is the heat exchange with the thermal bath and the second term is the mechanical work performed on the gas. In the second line, the third and the fourth terms are related to the interaction energy. The equation for ideal gases is recovered by setting $a = 0$ and $b = 0$.

III. EXCESS ENERGY CONSUMPTION

During the separation, mechanical work is performed by moving the membranes with the rate of energy consumption

$$\dot{W} = -p_L \dot{V}_L - p_M \dot{V}_M - p_R \dot{V}_R, \tag{4}$$

where the pressure p_k in each compartment is given by Eq. (1) and $\dot{V}_k = dV_k/dt$ is the volume change rate of compartment k. For convenience, we define two dimensionless parameters determining the configuration of the system: $x^L \equiv V_L/V_t$ and $x^R \equiv V_R/V_t$. Initially, the two species of molecules are completely mixed, with $x^L(0) = x^R(0) = 0$. Finally, they are separated, with $x^L(\tau)$ and $x^R(\tau)$ satisfying $x^L(\tau) + x^R(\tau) = 1$. Throughout the separation process, the volumes are subjected to a constraint condition $0 \leq x^L(t) + x^R(t) \leq 1$.

For quasistatic separation with infinite operation time, the minimum energy consumption is obtained as $W^{(0)}_{\rm min} = -N_t k_B T_0(\epsilon_\alpha \ln \epsilon_\alpha + \epsilon_\beta \ln \epsilon_\beta)$ by choosing the final volume proportional to the ratio $\epsilon_\sigma \equiv N_\sigma/N_t$ of the two gases, namely, $x^L(\tau) = \epsilon_\alpha$ and $x^R(\tau) = \epsilon_\beta$ when the van der Waals constant a satisfies $aN_t/V_t k_B T_0 \ll 1$. The proof is given in Appendix C. To complete the separation in finite time, excess energy consumption is required: $W_{\rm ex} \equiv W - W^{(0)}_{\rm min}$.

In the following, we focus on the separation processes where the control parameters are varied much more slowly than the relaxation timescales. For slow separation processes, the leading term of rate of excess energy consumption is expressed in a quadratic form:

$$\dot{W}_{\rm ex} = \begin{pmatrix} \dot{x}^L & \dot{x}^R \end{pmatrix} \Theta \Lambda^{-1} \Xi \begin{pmatrix} \dot{x}^L \\ \dot{x}^R \end{pmatrix}. \tag{5}$$

The three matrices, denoted by Θ, Λ, and Ξ, characterize the linear response of the system state to the external driving, the relaxation of a near-equilibrium state, and the change of the instantaneous equilibrium state, respectively. Detailed derivations of Eq. (5) and the expressions for the three matrices can be found in Appendix D. In this situation, thermodynamic geometry can be used to optimize the control schemes to reduce the energy consumption [45–48], and the control scheme with the minimum energy consumption in finite time is converted into searching for geodesic paths with the metric.

IV. RIEMANN GEOMETRY OF THE CONFIGURATION SPACE

The quadratic form of the rate of the excess energy consumption $\dot{W}_{\rm ex}$ allows the definition of a geometric length in the configuration space spanned by the control parameters (x^L, x^R). For the separation finished at finite operation time $t = \tau$ with $x^L(\tau) + x^R(\tau) = 1$, the protocol $x^L(t)$ and $x^R(t)$ is designed to minimize the excess energy consumption.

We define a metric G for the current Riemann manifold as

$$G \equiv \frac{\Theta \Lambda^{-1} \Xi + (\Theta \Lambda^{-1} \Xi)^T}{2} = \begin{pmatrix} g_{LL} & g_{LR} \\ g_{RL} & g_{RR} \end{pmatrix}. \tag{6}$$

For the case of ideal gases ($a = 0$ and $b = 0$), we obtain analytical expressions for the metric: $g_{LL} = N_t k_B T_0[\epsilon_\beta \tau_\beta (x^R)^2/(1-x^L)^3 + \epsilon_\alpha \tau_\alpha/(1-x^R) + 2/3 \times \epsilon_\beta^2 \tau_h/(1-x^L)^2]$, $g_{LR} = g_{RL} = N_t k_B T_0\{\epsilon_\alpha \tau_\alpha x^L/(1-x^R)^2 + \epsilon_\beta \tau_\beta x^R/(1-x^L)^2 + 2/3 \times \epsilon_\alpha \epsilon_\beta \tau_h/[(1-x^L)(1-x^R)]\}$, and $g_{RR} = N_t k_B T_0[\epsilon_\alpha \tau_\alpha (x^L)^2/(1-x^R)^3 + \epsilon_\beta \tau_\beta/(1-x^L) + 2/3 \times \epsilon_\alpha^2 \tau_h/(1-x^R)^2]$, where we have introduced the timescale of heat transfer $\tau_h \equiv 1/\gamma$ and that of particle transport of type-σ molecules $\tau_\sigma \equiv V_t/\kappa_\sigma k_B T_0 \mathcal{A}$. The details can be found in Appendix E.

With the Cauchy-Schwarz inequality $\int_0^\tau \dot{W}_{\rm ex} dt \int_0^\tau dt \geq (\int_0^\tau \sqrt{\dot{W}_{\rm ex}} dt)^2$, the excess energy consumption of different protocols for a given path $\mathcal{P}(x^L, x^R) = 0$ is bounded as

$$W_{\rm ex} \geq \frac{\mathcal{L}^2}{\tau}, \tag{7}$$

where the thermodynamic length $\mathcal{L} = \int_0^\tau \sqrt{\dot{W}_{\rm ex}} dt$ is determined only by the path in the configuration space [43,45,47]:

$$\mathcal{L} = \int_{\mathcal{P}} \sqrt{\begin{pmatrix} dx^L & dx^R \end{pmatrix} G \begin{pmatrix} dx^L \\ dx^R \end{pmatrix}}. \tag{8}$$

The equality in Eq. (7) holds for the protocol with constant excess energy consumption rate $\dot{W}_{\rm ex} = {\rm const}$. The task of seeking the minimum energy consumption in finite time is converted into identifying geodesic paths connecting the starting point $(0, 0)$ and the target point $(\epsilon_\alpha, \epsilon_\beta)$ in the configuration space.

Such geodesic paths in the current Riemann manifold are described by the geodesic equations,

$$\ddot{x}^k + \Gamma^k_{ij} \dot{x}^i \dot{x}^j = 0, \tag{9}$$

with boundary conditions $x^L(0) = x^R(0) = 0$ and $x^L(\tau) = \epsilon_\alpha, x^R(\tau) = \epsilon_\beta$. Here Einstein summation is used to simplify the summation of repeated indices. The Christoffel symbols Γ^k_{ij} are obtained as $\Gamma^k_{ij} = (1/2) g^{kl} \left(\partial g_{li}/\partial x^j + \partial g_{lj}/\partial x^i - \partial g_{ij}/\partial x^l\right)$, where g^{kl} are the elements of the inverse metric G^{-1}. For van der Waals gases, the Christoffel symbols are obtained numerically by calculation of the derivatives of the metric. For ideal gases, we obtain analytical results for the Christoffel symbols in Appendix E.

We remark that some singularities of the differential equations arise when solving the geodesic Eq. (9) and the

evolution Eqs. (2) and (3). We show numerical techniques for dealing with these singularities in Appendix F.

V. SYMMETRIC CONTROL PATH

As the first step, we optimize the separation along a symmetric path $x^L(t) = x^R(t) \equiv x(t)$ for the case where the two gases have equal particle numbers $N_\alpha = N_\beta$, and membranes A and B exhibit equivalent permeability, i.e., $\kappa_\alpha = \kappa_\beta$ (consequently $\tau_\alpha = \tau_\beta \equiv \tau_p$). We mainly discuss the analytically solvable case for ideal gases, which is rather typical to reflect the mechanism of membrane separation. The optimization for van der Waals gases is solved numerically to support the analytical result of ideal gas approximation. In the numerical calculation, we assume that the two mixed gases have identical van der Waals constants $a_k = a$ and $b_k = b$; this provides a symmetric setup in the dynamics of separation. The protocol $x(t)$ is optimized for lower excess energy consumption.

For ideal gases, we observe that the most straightforward symmetric linear protocol $x(t) = t/2\tau$ with excess energy consumption $W_{\rm ex}^{(\rm linear)} = N_t k_B T_0(\tau_h/3\tau + 3\tau_p/4\tau)$ does not satisfy the geodesic equation (9), indicating that such a linear protocol is not optimal under the symmetric setup. The thermodynamic length of the symmetric path $x^L(t) = x^R(t) = x(t)$ with starting point $x(0)$ and end point $x(\tau)$ is obtained explicitly by Eq. (8) as

$$\mathcal{L}_s(x(\tau)) = 2\sqrt{N_t k_B T_0}\left(\sqrt{\frac{\tau_p}{1-x} + \frac{2}{3}\tau_h} - \sqrt{\frac{2\tau_h}{3}}\sinh^{-1}\sqrt{\frac{2(1-x)\tau_h}{3\tau_p}}\right)\Bigg|_{x=0}^{x(\tau)}. \quad (10)$$

By setting $x(\tau) = 0.5$, we obtain the length of the whole symmetric path $\mathcal{L}_{\rm sym} = \mathcal{L}_s(0.5)$.

The lower bound of the excess energy consumption for the symmetric path is $\mathcal{L}_{\rm sym}^2/\tau$. To obtain such a bound, the parameters are controlled with the *optimal symmetric protocol* $x^{(\rm OSP)}(t)$ in an implicit form as

$$\mathcal{L}_s(x^{(\rm OSP)}(t)) = t\mathcal{L}_{\rm sym}/\tau. \quad (11)$$

We explicitly describe two cases where either the relaxation of particle transport or that of heat exchange dominates during the separation process:

(1) Particle-transport-dominated process ($\tau_h \ll \tau_p$). The temperature of the system is identical to that of the bath, $T = T_0$. The excess energy consumption rate is simplified as $\dot{W}_{\rm ex} = N_t k_B T_0 \tau_p (1-x)\{(d/dt)[x/(1-x)]\}^2$. The thermodynamic length follows as $\mathcal{L} = (2\sqrt{2}-2)\sqrt{N_t k_B T_0 \tau_p}$. According to Eq. (7), the minimum excess energy consumption is given by

$$W_{\rm ex}^{(\rm min)} = (12 - 8\sqrt{2})N_t k_B T_0 \frac{\tau_p}{\tau}. \quad (12)$$

TABLE I. Optimal symmetric protocol for equally mixed ideal gases. Two regions of the relaxation timescales are considered: (1) particle-transport-dominated process ($\tau_h \ll \tau_p$) and (2) heat-exchange-dominated process ($\tau_h \gg \tau_p$).

	$\tau_h \ll \tau_p$	$\tau_h \gg \tau_p$
$W_{\rm ex}^{(\rm min)}$	$(12-8\sqrt{2})N_t k_B T_0 \frac{\tau_p}{\tau}$	$\frac{2(\ln 2)^2}{3} N_t k_B T_0 \frac{\tau_h}{\tau}$.
Protocol	$x(t) = 1 - [(\sqrt{2}-1)t/\tau + 1]^{-2}$	$x(t) = 1 - 2^{-t/\tau}$

The optimal symmetric protocol to achieve the above minimum excess energy consumption is designed as follows;

$$x(t) = 1 - [(\sqrt{2}-1)t/\tau + 1]^{-2}. \quad (13)$$

(2) Heat-exchange-dominated process ($\tau_h \gg \tau_p$). The excess energy consumption rate is simplified to $\dot{W}_{\rm ex} = 2/3 \times N_t k_B T_0 \tau_h \dot{x}^2/(1-x)^2$. The minimum excess energy consumption is given by

$$W_{\rm ex}^{(\rm min)} = \frac{2(\ln 2)^2}{3} N_t k_B T_0 \frac{\tau_h}{\tau}. \quad (14)$$

The optimal symmetric protocol is obtained as follows:

$$x(t) = 1 - 2^{-t/\tau}. \quad (15)$$

We summarize the two cases in Table I.

To validate our analytical results for the optimal symmetric protocol, we perform numerical simulations. We consider a symmetric situation of 2 mol of equally mixed gases at room temperature $T_0 = 298.15$ K. With regard to the particle numbers of the two gases, $N_\alpha = N_\beta = N_A$, where $N_A = 6.022 \times 10^{23}\ \mathrm{mol}^{-1}$ is the Avogadro constant. The total volume is chosen as $V_t = 0.04893\ \mathrm{m}^3$ to ensure that the initial pressure is atmospheric pressure. For van der Waals gases, we set $aN_t/V_t k_B T_0 = 0.04$ and $N_t b/V_t = 0.02$ throughout the rest of this paper. The corresponding values of a and b are about 20 times their values for O_2. We choose relatively large van der Waals constants to distinguish the results from those for ideal gases. With the values of a and b for O_2, the results for van der Waals gases are almost the same as those for ideal gases. Therefore, the ideal gas approximation works well for the current conditions of pressure and temperature.

The numerical results for the optimal symmetric protocols are shown in Figs. 2(a), 2(c), and 2(e), and the numerical results for the excess energy consumption are shown in Figs. 2(b), 2(d), and 2(f). The relaxation timescales are set as $\tau_p = 1$ s and $\tau_h = 0.01$ s in Figs. 2(a) and 2(b) for the particle-transport-dominated processes, $\tau_p = 1$ s and $\tau_h = 1$ s in Figs. 2(c) and 2(d) for the intermediate case, and $\tau_p = 0.01$ s and $\tau_h = 1$ s in Figs. 2(e) and 2(f) for the heat-exchange-dominated processes. In Figs. 2(a), 2(c), and 2(e), the optimal symmetric protocols for ideal gases

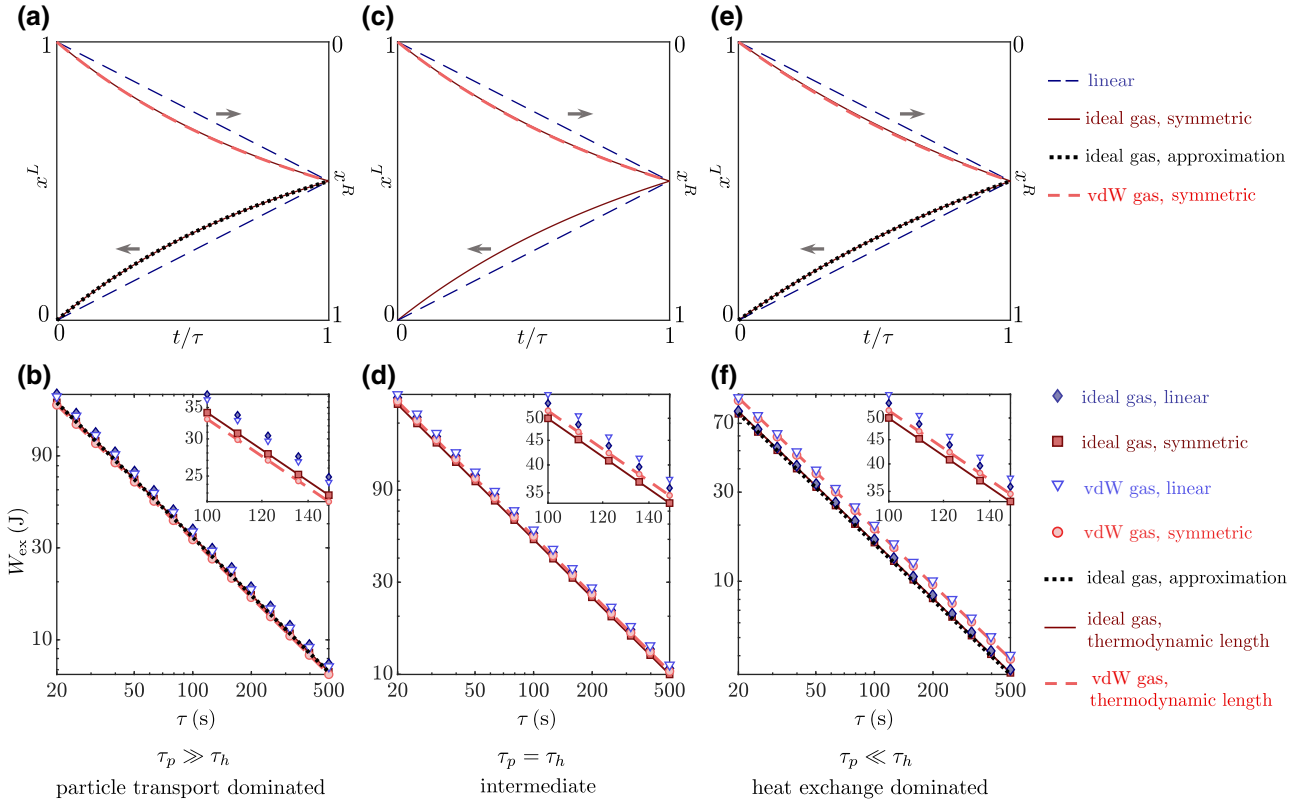

FIG. 2. Symmetric protocols and excess energy consumption on the symmetric path for ideal gases and van der Waals (vdW) gases. The relaxation timescales are set to $\tau_p = 1$ s and $\tau_h = 0.01$ s in (a),(b), $\tau_p = 1$ s and $\tau_h = 1$ s in (c),(d), and $\tau_p = 0.01$ s and $\tau_h = 1$ s in (e),(f). (a),(c),(e) The optimal symmetric protocols for ideal gases (solid dark-red curve) and van der Waals gases (dashed light-red curves). The dotted black curves in (a),(c) indicate the analytical optimal symmetric protocols (13) and (15) in the two limits, and the dashed blue line represents the linear protocol. (b),(d),(f) The excess energy consumption. The markers show the excess energy consumption obtained by numerically solving the evolution equations (2) and (3) under the given protocols, with squares (circles) indicating ideal gases (van der Waals gases) under the optimal symmetric protocol, and diamonds (triangles) indicating ideal gases (van der Waals gases) under the linear protocol. The bounds (12) and (14) of the excess energy consumption are shown by the dotted black lines in (b),(f), respectively.

analytically expressed in Eqs. (10) and (11) are represented by the solid dark-red curves, and those of the van der Waals gases are represented by the dashed light-red curves by numerically solving the geodesic equation (9). The explicit optimal symmetric protocols (13) and (15) in the two limits are shown by the dotted black curves in Figs. 2(a) and 2(e). The linear protocol of the separation is given by the dashed blue line.

The numerical results for the excess energy consumption for the optimal symmetric protocols and the linear protocol are presented in Figs. 2(b), 2(d), and 2(f). Specifically, we use markers to depict the excess energy consumption obtained by numerically solving the evolution equations (2) and (3) under the given protocols, while the lines represent the predictions with use of the thermodynamic lengths via the bounds in Eqs. (12) and (14).

From these figures, there are two noteworthy observations. Firstly, the optimal control protocol with reduced energy consumption differs from the simplistic linear protocol. This discrepancy underscores the necessity to search for an even better control protocol. Secondly, the implementation of the ideal gas approximation yields a commendable estimation of the energy consumption associated with the separation of real gases. Despite the ideal gas model's inherent simplifications and assumptions, it remarkably captures the essential aspects of the energy requirements in real gas separation processes.

VI. SYMMETRY BREAKING IN THE OPTIMAL SEPARATION PROTOCOL

The question arises of whether the symmetric protocol is the optimal one with the minimum energy consumption. Our answer is it is not. We find two symmetry-breaking protocols to obtain the minimum energy consumption for the perfectly symmetric setup.

For given parameters, we use the shooting method [54] to numerically search for the geodesic path connecting the starting point $(0, 0)$ and the target point $(0.5, 0.5)$ in the configuration space. In such a method, the problem of

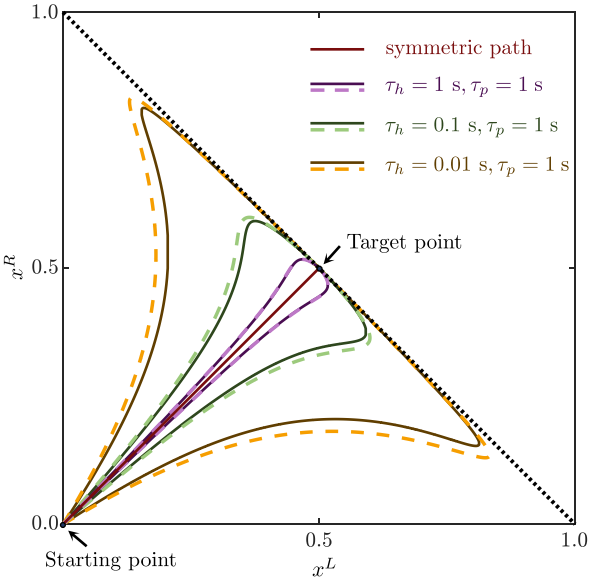

FIG. 3. Optimal symmetry-breaking protocols with the minimum excess energy consumption for the separation process. The permeability of membranes A and B with regard to the corresponding type of molecule is identical, and the numbers of type-α and type-β molecules are equal. Results are shown for three cases with different relaxation timescales ($\tau_h = 1$ s and $\tau_p = 1$ s, $\tau_h = 0.1$ s and $\tau_p = 1$ s, and $\tau_h = 0.01$ s and $\tau_p = 1$ s) for both ideal gases (solid curves) and van der Waals gases (dashed curves).

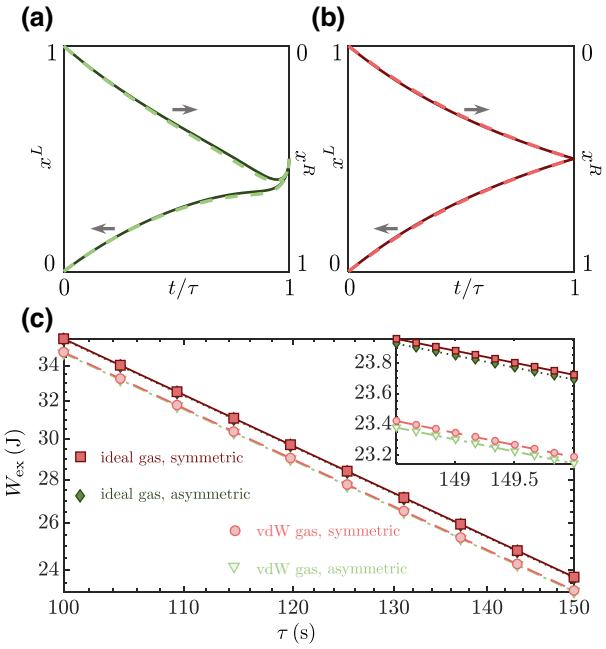

FIG. 4. Comparison of optimal symmetry-breaking and optimal symmetric protocols. (a),(b) The control schemes for these protocols, with solid curves representing protocols for ideal gases and dashed curves representing protocols for van der Waals (vdW) gases. (c) Excess energy consumption W_{ex} versus operation time τ. For ideal gases, squares and diamonds represent the excess energy consumption under the optimal symmetric and optimal symmetry-breaking protocols, respectively. For van der Waals gases, circles and triangles represent the excess energy consumption under the optimal symmetric and optimal symmetry-breaking protocols, respectively. The dotted dark-green line (dash-dotted light-green line) represents the excess energy consumption predicted by the thermodynamic length $W_{ex} = \mathcal{L}^2/\tau$ under the optimal symmetry-breaking protocols for ideal gases (van der Waals gases), while the solid dark-red line (dashed light-red line) shows the excess energy consumption under the optimal symmetric protocols for ideal gases (van der Waals gases).

finding the geodesic path connecting two points is converted into a problem of finding the proper initial value of the velocity $\dot{x}^L(0)$ and $\dot{x}^R(0)$ in Eq. (9) with starting point $x^L(0) = x^R(0) = 0$ to meet the condition $x^L(\tau) = x^R(\tau) = 0.5$. We consider three cases that involve different sets of relaxation timescales: $\tau_h = 1$ s and $\tau_p = 1$ s; $\tau_h = 0.1$ s and $\tau_p = 1$ s; and $\tau_h = 0.01$ s and $\tau_p = 1$ s. In Fig. 3, we identify three geodesic paths for each case, including one symmetric path and two symmetry-breaking paths. The solid curves show the results for ideal gases, and the dashed curves show the results for van der Waals gases. The symmetric geodesic path is shown as a solid red line. To visualize the symmetry breaking of the control scheme in the optimal separation protocol, we sketch the three-dimensional embedding of the current two-dimensional Riemann manifold in Fig. 1(b), where the thermodynamic length is reflected by the length of the path. The symmetry-breaking curves are shorter than the symmetric curve, representing a smaller excess energy consumption.

Figure 4 shows the excess energy consumption of the optimal symmetry-breaking protocol for the case with $\tau_h = 0.1$ s and $\tau_p = 1$ s. Similar results for other parameter combinations are not shown here. The optimal symmetry-breaking protocol and the optimal symmetric protocol are given in Figs. 4(a) and 4(b) as solid curves for ideal gases and dashed curves for van der Waals gases. In the optimal symmetry-breaking protocol, the two membranes approach each other at a position different from the equilibrium position, and then they are moved together to the equilibrium position. In Fig. 4(c), we compare the excess energy consumption in the optimal symmetry-breaking protocol and the optimal symmetric protocol. The markers show the excess energy consumption obtained by numerically solving the evolution equations (2) and (3) under the given protocols, while the lines show the predictions with use of the thermodynamic lengths. The thermodynamic lengths are $\mathcal{L}^{\text{ideal}}_{\text{sym}} = 59.66\ (\text{J s})^{1/2}$ and $\mathcal{L}^{\text{ideal}}_{\text{asym}} = 59.61\ (\text{J s})^{1/2}$ for ideal gases and $\mathcal{L}^{\text{vdW}}_{\text{sym}} = 58.98\ (\text{J s})^{1/2}$ and $\mathcal{L}^{\text{vdW}}_{\text{asym}} = 58.92\ (\text{J s})^{1/2}$ for van der Waals gases. The lengths of the optimal symmetry-breaking green geodesic paths are shorter than those of the symmetric paths.

VII. DISCUSSION

We established the equivalence between optimizing control strategies to minimize energy consumption and identifying geodesic paths within a Riemann space, a relationship that has been effectively leveraged in optimizing control protocols in stochastic and quantum thermodynamics [45–49]. By using this equivalence, we demonstrated that the minimum energy consumption is directly proportional to the square of the geodesic path's length and inversely proportional to the duration τ of the operation.

For separation processes with a perfectly symmetric setup ($\tau_\alpha = \tau_\beta = \tau_p$, $\epsilon_\alpha = \epsilon_\beta = 0.5$, $a_\alpha = a_\beta = a$, and $b_\alpha = b_\beta = b$), we found three geodesic paths. One of the geodesic paths aligns with our intuitive expectation as a symmetric straight line in the configuration space (x^L, x^R). We optimized the excess energy consumption along this path and obtained a symmetric yet nonlinear optimal protocol. Specially, under the approximation of ideal gases, we predict that the complete separation of equally mixed single-atom ideal gases requires an excess energy consumption of at least $(12 - 8\sqrt{2})N_t k_B T_0 \tau_p/\tau$ for a particle-transport-dominated process and $2(\ln 2)^2 N_t k_B T_0 \tau_h/3\tau$ for a heat-exchange-dominated process, where τ_p and τ_h are the relaxation timescales for particle transport and heat exchange, respectively.

The other two symmetric-breaking geodesic paths are proved to achieve the minimal thermodynamic length. The corresponding symmetry-breaking protocols are optimal and achieve the lowest energy consumption for a given operation time τ. In such protocols, one membrane is moved faster than the other, the membranes approach each other at a position slightly different from the equilibrium position, and then they are moved together to the equilibrium position. The topic of reducing energy consumption is becoming increasingly crucial. We believe our geometry method is an auspicious beginning to optimize the cost of the industrial membrane separation protocols.

ACKNOWLEDGMENTS

This work was supported by the National Natural Science Foundation of China (Grants No. 12088101, No. 11534002, No. 11875049, No. U1930402, No. U1930403, and No. 12047549) and the National Basic Research Program of China (Grant No. 2016YFA0301201).

J.-F.C. and R.-X.Z. contributed equally to this work.

APPENDIX A: DERIVATION OF THE REVISED FICK'S LAW OF DIFFUSION FOR VAN DER WAALS GASES

Here we derive the revised Fick's law given in Eq. (2). For ideal gases, Fick's law of diffusion asserts that the flux of a certain particle across a membrane is proportional to the density difference of that particle. If we take type-α molecules as an example, the flux is expressed as

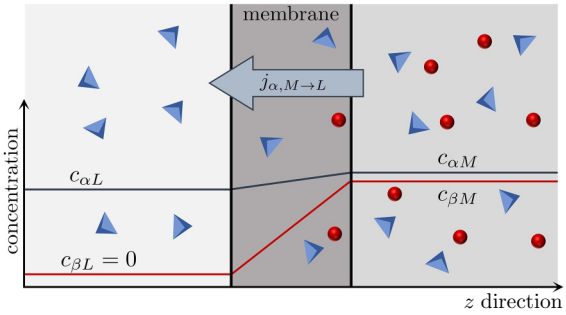

FIG. 5. Particle transport across the membrane from the middle compartment to the left compartment. The flux density is denoted as $j_{\alpha,M\to L}$.

$$\frac{J^{(\mathrm{ideal})}_{\alpha,M\to L}}{\kappa_\alpha \mathcal{A} k_B T} = c_{\alpha M} - c_{\alpha L}. \tag{A1}$$

In the equilibrium state, the flux is zero, $J^{(\mathrm{ideal})}_{\alpha,M\to L} = 0$, and the particle density of type-α molecules across membrane A is the same, $c_{\alpha M} = c_{\alpha L}$. However, for mixed van der Waals gases, the same particle density does not lead to an identical chemical potential, which is the necessary condition of equilibrium. Thus, Fick's law of diffusion should be revised for van der Waals gases.

We denote the diffusion flux of molecules (type α) over membrane A from the middle compartment to the left compartment as $J_{\alpha,M\to L} \equiv \dot{N}_{\alpha L} = j_{\alpha,M\to L}\mathcal{A}$, where $j_{\alpha,M\to L}$ is the flux density and $\mathcal{A}$ is the area of the membrane. The diagram is illustrated in Fig. 5. The flux $J_{\alpha,M\to L}$ is driven by the chemical potential difference $\Delta\mu_\alpha = \mu_{\alpha M} - \mu_{\alpha L}$. The chemical potential of type-σ molecules in compartment k is given by

$$\mu_{\sigma k} = \frac{\partial F_k}{\partial N_{\sigma k}}, \tag{A2}$$

where the free energy F_k for gas molecules in each compartment is given later.

We consider the simple case with the chemical gradient $-\partial_z \mu_\alpha(z)$ along the z direction over membrane A. The force $-\partial_z \mu_\alpha(z)$ induced by the chemical potential gradient is balanced by a friction force $-k v_\alpha$ across the membrane as

$$-\partial_z \mu_\alpha(z) - k v_\alpha = 0, \tag{A3}$$

where v_α is the drift velocity of type-α molecules. The drift velocity is related to the flux density $j_{\alpha,M\to L} = c_\alpha v_\alpha$ through the density $c_\alpha(z)$. Solving the steady flux density

j_α from Eq. (A3), we obtain

$$j_{\alpha,M\to L} = -\frac{c_\alpha}{k}\frac{\partial \mu_\alpha(z)}{\partial z}. \tag{A4}$$

The free energy for the gas molecules in the chamber is given by $F = F_M + F_L + F_R$. The free energy F_M of the gases in the middle compartment is given by

$$\begin{aligned} F_M = &-N_M k_B T\left[\frac{3}{2}\ln\left(\frac{2\pi m k_B T}{h^2}\right)+1\right] \\ &- a\frac{N_M^2}{V_M} - k_B T\left(N_{\alpha M}\ln\frac{V_M - N_M b}{N_{\alpha M}}\right. \\ &\left. + N_{\beta M}\ln\frac{V_M - N_M b}{N_{\beta M}}\right), \end{aligned} \tag{A5}$$

where m is the mass of a single molecule and h is the volume of the phase-space grid. Similarly, the free energies of the gases in the left and right compartments are

$$\begin{aligned} F_L = &-N_{\alpha L} k_B T\left[\frac{3}{2}\ln\left(\frac{2\pi m k_B T}{h^2}\right)+1\right] \\ &- a\frac{N_{\alpha L}^2}{V_L} - N_{\alpha L} k_B T\ln\frac{V_L - N_{\alpha L} b}{N_{\alpha L}}, \end{aligned} \tag{A6}$$

$$\begin{aligned} F_R = &-N_{\beta R} k_B T\left[\frac{3}{2}\ln\left(\frac{2\pi m k_B T}{h^2}\right)+1\right] \\ &- a\frac{N_{\beta R}^2}{V_R} - N_{\beta R} k_B T\ln\frac{V_R - N_{\beta R} b}{N_{\beta R}}. \end{aligned} \tag{A7}$$

The chemical potentials of the gases in different compartments are obtained from $\mu_{\sigma k} = \partial F_k/\partial N_{\sigma k}$ as

$$\begin{aligned} \mu_{\alpha M} = &-\frac{3}{2}k_B T\ln\left(\frac{2\pi m k_B T}{h^2}\right) - 2a\frac{N_M}{V_M} \\ &+ k_B T\left(\frac{N_M b}{V_M - N_M b} - \ln\frac{V_M - N_M b}{N_{\alpha M}}\right) \\ \simeq &-\frac{3}{2}k_B T\ln\left(\frac{2\pi m k_B T}{h^2}\right) + k_B T\ln c_{\alpha M} \\ &+ 2\left(b k_B T - a\right)\left(c_{\alpha M} + c_{\beta M}\right), \end{aligned} \tag{A8}$$

$$\begin{aligned} \mu_{\alpha L} = &-\frac{3}{2}k_B T\ln\left(\frac{2\pi m k_B T}{h^2}\right) - 2a\frac{N_{\alpha L}}{V_L} \\ &+ k_B T\left(\frac{N_{\alpha L} b}{V_L - N_{\alpha L} b} - \ln\frac{V_L - N_{\alpha L} b}{N_{\alpha L}}\right) \\ \simeq &-\frac{3}{2}k_B T\ln\left(\frac{2\pi m k_B T}{h^2}\right) + k_B T\ln c_{\alpha L} \\ &+ 2\left(b k_B T - a\right) c_{\alpha L}. \end{aligned} \tag{A9}$$

To the first order of the van der Waals constants, the flux density is given by

$$j_{\alpha,M\to L} = -\frac{k_B T}{k}\left[\frac{\partial c_\alpha}{\partial z} + 2(b - \frac{a}{k_B T})c_\alpha\left(\frac{\partial c_\alpha}{\partial z} + \frac{\partial c_\beta}{\partial z}\right)\right]. \tag{A10}$$

For the small density difference $\Delta c_\alpha = c_{\alpha M} - c_{\alpha L}$ across membrane A with thickness d, we use the substitutions $\partial c_\alpha/\partial z \to (c_{\alpha M} - c_{\alpha L})/d$, $c_\alpha \to (c_{\alpha M} + c_{\alpha L})/2$, and $\partial c_\beta/\partial z \to (c_{\beta M} - c_{\beta L})/d$, with $c_{\beta L} = 0$. The flux density is rewritten as

$$j_{\alpha,M\to L} \approx \frac{k_B T}{kd}\left[c_{\alpha M} - c_{\alpha L} + \left(b - \frac{a}{k_B T}\right)c_{\beta M}(c_{\alpha M} + c_{\alpha L})\right]. \tag{A11}$$

By defining $\kappa = 1/kd$, we obtain a revised Fick's law for van der Waals gases:

$$\frac{J_{\alpha,M\to L}}{\kappa_\alpha \mathcal{A} k_B T} = c_{\alpha M} - c_{\alpha L} + \left(b - \frac{a}{k_B T}\right)c_{\beta M}(c_{\alpha M} + c_{\alpha L}). \tag{A12}$$

For the case with $a = 0$ and $b = 0$, Fick's law for ideal gases is recovered as $J_{\alpha,M\to L} = \kappa_\alpha \mathcal{A} k_B T(c_{\alpha M} - c_{\alpha L})$.

APPENDIX B: DERIVATION OF THE TEMPERATURE EVOLUTION

Here we derive the differential equation (3) that determines the evolution of gas temperature. We write the first law of thermodynamics for the gases in each compartment as

$$\begin{aligned} dU_L &= dQ_L - p_L dV_L + u_{\alpha L} dN_{\alpha L}, \\ dU_M &= dQ_M - p_M dV_M + u_{\alpha M} dN_{\alpha M} + u_{\beta M} dN_{\beta M}, \\ dU_R &= dQ_R - p_R dV_R + u_{\beta R} dN_{\beta R}, \end{aligned} \tag{B1}$$

where $u_{\sigma k}$ is the partial molar internal energy of the gases in each compartment. For van der Waals gases, the internal energy in each compartment is given by $U_k = 3N_k k_B T/2 - aN_k^2/V_k$, and the partial molar internal energy $u_{\sigma k}$ is explicitly given by

$$\begin{aligned} u_{\alpha L} &= \frac{\partial U_L}{\partial N_\alpha} = \frac{3}{2}k_B T - \frac{2aN_{\alpha L}}{V_L}, \\ u_{\alpha M} &= \frac{\partial U_M}{\partial N_\alpha} = \frac{3}{2}k_B T - \frac{2a\left(N_{\alpha M} + N_{\beta M}\right)}{V_M}, \\ u_{\beta M} &= \frac{\partial U_M}{\partial N_\beta} = \frac{3}{2}k_B T - \frac{2a\left(N_{\alpha M} + N_{\beta M}\right)}{V_M}, \\ u_{\beta R} &= \frac{\partial U_M}{\partial N_\beta} = \frac{3}{2}k_B T - \frac{2aN_{\beta R}}{V_R}, \end{aligned} \tag{B2}$$

and the differences are caused by interaction energy

$$u_{\alpha L}-u_{\alpha M}=-\frac{2aN_{\alpha L}}{V_L}+\frac{2a\left(N_{\alpha M}+N_{\beta M}\right)}{V_M},$$
$$u_{\beta R}-u_{\beta M}=-\frac{2aN_{\beta R}}{V_R}+\frac{2a\left(N_{\alpha M}+N_{\beta M}\right)}{V_M}. \tag{B3}$$

With the identical gas temperature T, we can sum over the three expressions in Eq. (B1) and obtain the differential equation

$$\dot{U}=\dot{Q}-p_L\dot{V}_L-p_M\dot{V}_M-p_R\dot{V}_R+u_{\alpha L}\dot{N}_{\alpha L}+u_{\alpha M}\dot{N}_{\alpha M}+u_{\beta M}\dot{N}_{\beta M}+u_{\beta R}\dot{N}_{\beta R}. \tag{B4}$$

Plugging the internal energy $U=\sum_{k=L,M,R}U_k=3N_tk_BT/2-a\sum_{k=L,M,R}N_k^2/V_k$, the heat exchange $\dot{Q}=-C_V\gamma(T-T_0)$ by Newton's law of cooling, the pressures $p_k=N_kk_BT/(V_k-N_kb)-aN_k^2/V_k^2$ of van der Waals gases, and the partial molar internal energy $u_{\sigma k}$ into Eq. (B2), and using the constraints $\dot{N}_{\beta M}=-\dot{N}_{\beta R}$ and $\dot{N}_{\alpha M}=-\dot{N}_{\alpha L}$ of particle numbers, we obtain the differential equation (3) to describe the evolution of the gas temperature.

APPENDIX C: MINIMUM ENERGY CONSUMPTION IN QUASISTATIC SEPARATION OF VAN DER WAALS GASES

To obtain the energy consumption in quasistatic separation, we use the normal formula $W^{(0)}=\Delta F=F^f-F^i$ from the free-energy change of van der Waals gases in the middle compartment. Notice that the gases are initially prepared in the middle compartment ($V_L^i=0$, $V_R^i=0$, $V_M^i=V_t$) and are finally separated in the left and right compartments ($V_L^f+V_R^f=V_t$, $V_M^f=0$). Using Eqs. (A5)–(A7), we find the work in quasistatic separation is explicitly given as

$$W^{(0)}=-k_BT_0\left(N_\alpha\ln\frac{V_L^f-N_\alpha b}{V_t-N_tb}+N_\beta\ln\frac{V_R^f-N_\beta b}{V_t-N_tb}\right)+a\left(\frac{N_t^2}{V_t}-\frac{N_\alpha^2}{V_L^f}-\frac{N_\beta^2}{V_R^f}\right). \tag{C1}$$

One can prove that the minimum quasistatic energy consumption $W_{\min}^{(0)}=-N_tk_BT_0(\epsilon_\alpha\ln\epsilon_\alpha+\epsilon_\beta\ln\epsilon_\beta)$ is obtained at the optimal position $V_L^f=V_tN_\alpha/N_t$ and $V_R^f=V_tN_\beta/N_t$ for the small van der Waals constants a and b that satisfy

$$2\left(1-\frac{N_tb}{V_t}\right)^2\frac{aN_t}{V_tk_BT_0}<1. \tag{C2}$$

If we choose the optimal position, the system at the end of the quasistatic separation is in both thermal equilibrium and mechanical equilibrium.

APPENDIX D: DERIVATION OF THE EXCESS ENERGY CONSUMPTION RATE

Here we derive Eq. (5) and the expressions for the three matrices Θ, Λ, and Ξ. For convenience, we rewrite Eqs. (2) and (3) in a compact form:

$$\dot{N}_{\alpha L}=J_1(N_{\alpha L},N_{\beta R},T,V_L,V_R), \tag{D1}$$
$$\dot{N}_{\beta R}=J_2(N_{\alpha L},N_{\beta R},T,V_L,V_R), \tag{D2}$$
$$\dot{T}=J_3(N_{\alpha L},N_{\beta R},T,V_L,V_R), \tag{D3}$$

where the first two fluxes $J_1\equiv J_{\alpha,M\to L}$ and $J_2\equiv J_{\beta,M\to R}$ correspond to particle transport, and the third flux J_3 is given by the right-hand side of Eq. (3). The molecule numbers $N_{\alpha L}$ and $N_{\beta R}$ and the gas temperature T characterize the states of the gases in each compartment, and the volumes V_L and V_R are control parameters. In a quasistatic separation process, the particle numbers $N_{\alpha L}^{(0)}$ and $N_{\beta R}^{(0)}$ and the gas temperature $T^{(0)}=T_0$ are obtained by setting $J_l=0$ ($l=1,2,3$).

For the slow process, we can linearize the differential equations (D1)–(D3) by expanding the particle numbers and the gas temperature around their values for the quasistatic process as

$$N_{\alpha L}=N_{\alpha L}^{(0)}+N_{\alpha L}^{(1)}, \tag{D4}$$
$$N_{\beta R}=N_{\beta R}^{(0)}+N_{\beta R}^{(1)}, \tag{D5}$$
$$T=T_0+T^{(1)}. \tag{D6}$$

The finite-time corrections $N_{\alpha L}^{(1)}$, $N_{\beta R}^{(1)}$, and $T^{(1)}$ satisfy the linearized equations

$$\begin{pmatrix}\dot{N}_{\alpha L}^{(1)}\\ \dot{N}_{\beta R}^{(1)}\\ \dot{T}^{(1)}\end{pmatrix}=\begin{pmatrix}-\dot{N}_{\alpha L}^{(0)}\\ -\dot{N}_{\beta R}^{(0)}\\ J_3^{(0)}\end{pmatrix}-\Lambda\begin{pmatrix}N_{\alpha L}^{(1)}\\ N_{\beta R}^{(1)}\\ T^{(1)}\end{pmatrix}, \tag{D7}$$

where the third flux $J_3^{(0)}$ according to Eq. (3) is explicitly given as

$$J_3^{(0)}=J_3(N_{\alpha L}^{(0)},N_{\beta R}^{(0)},T_0,V_L,V_R) \tag{D8}$$
$$=-\frac{2T_0}{3N_t}\sum_{k=L,M,R}\frac{N_k^{(0)}\dot{V}_k}{V_k-N_k^{(0)}b}. \tag{D9}$$

The relaxation matrix Λ is related to the partial derivatives of the fluxes J_l as

$$\Lambda=-\begin{pmatrix}\frac{\partial J_1}{\partial N_{\alpha L}} & \frac{\partial J_1}{\partial N_{\beta R}} & \frac{\partial J_1}{\partial T}\\ \frac{\partial J_2}{\partial N_{\alpha L}} & \frac{\partial J_2}{\partial N_{\beta R}} & \frac{\partial J_2}{\partial T}\\ \frac{\partial J_3}{\partial N_{\alpha L}} & \frac{\partial J_3}{\partial N_{\beta R}} & \frac{\partial J_3}{\partial T}\end{pmatrix}\Bigg|_{(0)}, \tag{D10}$$

where the subscript (0) denotes the particle numbers $N_{\alpha L}$ and $N_{\beta R}$ and the temperature T take their values in a quasistatic process. In the following, the quantities for the middle compartment are rewritten with variables for the left and right compartments, i.e., $N_M^{(0)} = N_\alpha - N_{\alpha L}^{(0)} + N_\beta - N_{\beta R}^{(0)}$ and $\dot{V}_M = -\dot{V}_L - \dot{V}_R$.

According to Eq. (D7), the finite-time corrections for slow separation processes are obtained as

$$\begin{pmatrix} N_{\alpha L}^{(1)} \\ N_{\beta R}^{(1)} \\ T^{(1)} \end{pmatrix} = \Lambda^{-1} \begin{pmatrix} -\dot{N}_{\alpha L}^{(0)} \\ -\dot{N}_{\beta R}^{(0)} \\ J_3^{(0)} \end{pmatrix}, \tag{D11}$$

with Λ^{-1} the inverse of the relaxation matrix. A detailed introduction to the perturbation method can be found in Ref. [47] and also in the supplemental material in Ref. [55]. Two terms related to particle changes $\dot{N}_{\alpha L}^{(0)}$ and $\dot{N}_{\beta R}^{(0)}$ are obtained from the implicit function theorem as

$$\begin{pmatrix} -\dot{N}_{\alpha L}^{(0)} \\ -\dot{N}_{\beta R}^{(0)} \end{pmatrix} = M_1^{-1} M_2 \begin{pmatrix} \dot{V}_L \\ \dot{V}_R \end{pmatrix}, \tag{D12}$$

where the matrices M_1 and M_2 are explicitly expressed as

$$M_1 = \begin{pmatrix} \frac{\partial J_1}{\partial N_{\alpha L}} & \frac{\partial J_1}{\partial N_{\beta R}} \\ \frac{\partial J_2}{\partial N_{\alpha L}} & \frac{\partial J_2}{\partial N_{\beta R}} \end{pmatrix}\Bigg|_{(0)}, \quad M_2 = \begin{pmatrix} \frac{\partial J_1}{\partial V_L} & \frac{\partial J_1}{\partial V_R} \\ \frac{\partial J_2}{\partial V_L} & \frac{\partial J_2}{\partial V_R} \end{pmatrix}\Bigg|_{(0)}. \tag{D13}$$

With Eqs. (D9) and (D12), we can write the right-hand-side of Eq. (D11) into a compact form:

$$\begin{pmatrix} -\dot{N}_{\alpha L}^{(0)} \\ -\dot{N}_{\beta R}^{(0)} \\ J_3^{(0)} \end{pmatrix} = \Xi \begin{pmatrix} \dot{x}_L \\ \dot{x}_R \end{pmatrix}, \tag{D14}$$

where we use $x^L = V_L/V_t$ and $x^R = V_R/V_t$ to represent the control parameters.

The energy consumption for the finite-time process is given by Eq. (4). The quasistatic energy consumption rate $\dot{W}^{(0)} = -p_L^{(0)}\dot{V}_L - p_M^{(0)}\dot{V}_M - p_R^{(0)}\dot{V}_R$ is defined. The excess energy consumption rate $\dot{W}_{\rm ex} = \dot{W} - \dot{W}^{(0)}$ is obtained as

$$\dot{W}_{\rm ex} = \begin{pmatrix} \dot{x}^L & \dot{x}^R \end{pmatrix} \Theta \begin{pmatrix} N_{\alpha L}^{(1)} \\ N_{\beta R}^{(1)} \\ T^{(1)} \end{pmatrix}, \tag{D15}$$

where each element in the matrix Θ is explicitly expressed as follows:

$$\Theta_{11} = -V_t \sum_{k=L,M} \left(\frac{k_B T_0 V_k}{(V_k - N_k^{(0)} b)^2} - 2a \frac{N_k^{(0)}}{V_k^2} \right), \tag{D16}$$

$$\Theta_{12} = -V_t \left(\frac{k_B T_0 V_M}{(V_M - N_M^{(0)} b)^2} - 2a \frac{N_M^{(0)}}{V_M^2} \right), \tag{D17}$$

$$\Theta_{13} = -V_t \left(\frac{k_B N_{\alpha L}^{(0)}}{V_L - N_{\alpha L}^{(0)} b} - \frac{k_B N_M^{(0)}}{V_M - N_M^{(0)} b} \right), \tag{D18}$$

$$\Theta_{21} = -V_t \left(\frac{k_B T_0 V_M}{(V_M - N_M^{(0)} b)^2} - 2a \frac{N_M^{(0)}}{V_M^2} \right), \tag{D19}$$

$$\Theta_{22} = -V_t \sum_{k=M,R} \left(\frac{k_B T_0 V_k}{(V_k - N_k^{(0)} b)^2} - 2a \frac{N_k^{(0)}}{V_k^2} \right), \tag{D20}$$

$$\Theta_{23} = -V_t \left(\frac{k_B N_{\beta R}^{(0)}}{V_R - N_{\beta R}^{(0)} b} - \frac{k_B N_M^{(0)}}{V_M - N_M^{(0)} b} \right). \tag{D21}$$

We finally obtain the expression [Eq. (5)] for the excess energy consumption rate.

APPENDIX E: RESULTS FOR IDEAL GASES

We present several analytical results for ideal gases. The case of ideal gases is recovered by setting $a = 0$ and $b = 0$. The three matrices Θ, Λ, and Ξ are obtained analytically as

$$\Xi = \begin{pmatrix} -\frac{N_\alpha}{1-x^R} & -\frac{N_\alpha x^L}{(1-x^R)^2} \\ -\frac{N_\beta x^R}{(1-x^L)^2} & -\frac{N_\beta}{1-x^L} \\ \frac{2T_0}{3N_t}\frac{N_\beta}{1-x^L} & \frac{2T_0}{3N_t}\frac{N_\alpha}{1-x^R} \end{pmatrix}, \tag{E1}$$

$$\Theta = \begin{pmatrix} -\frac{(1-x^R)k_B T_0}{x^L(1-x^L-x^R)} & -\frac{k_B T_0}{1-x^L-x^R} & \frac{k_B N_\beta}{1-x^L} \\ -\frac{k_B T_0}{1-x^L-x^R} & -\frac{(1-x^L)k_B T_0}{x^R(1-x^L-x^R)} & \frac{k_B N_\alpha}{1-x^R} \end{pmatrix}, \tag{E2}$$

and

$$\Lambda = \begin{pmatrix} \frac{\kappa_\alpha \mathcal{A} k_B T_0 (1-x^R)}{V_t x^L (1-x^L-x^R)} & 0 & 0 \\ 0 & \frac{\kappa_\alpha \mathcal{A} k_B T_0 (1-x^L)}{V_t x^R (1-x^L-x^R)} & 0 \\ 0 & 0 & \gamma \end{pmatrix}. \tag{E3}$$

The excess energy consumption rate, according to Eq. (5), is simplified to

$$\begin{aligned} \dot{W}_{\rm ex} = {} & \frac{2N_t k_B T_0}{3\gamma} \left[\frac{\epsilon_\alpha \dot{x}^R}{1-x^R} + \frac{\epsilon_\beta \dot{x}^L}{1-x^L} \right]^2 \\ & + \frac{N_t V_t}{\mathcal{A}} \left\{ \frac{\epsilon_\alpha (1-x^R)}{\kappa_\alpha} \left[\frac{d}{dt} \left(\frac{x^L}{1-x^R} \right) \right]^2 \right. \\ & \left. + \frac{\epsilon_\beta (1-x^L)}{\kappa_\beta} \left[\frac{d}{dt} \left(\frac{x^R}{1-x^L} \right) \right]^2 \right\}, \end{aligned} \tag{E4}$$

where $\epsilon_\alpha = N_\alpha/N_t$ and $\epsilon_\beta = N_\beta/N_t$.

By introducing the timescale of heat transfer $\tau_h \equiv 1/\gamma$ and that of particle transport of type-σ molecules $\tau_\sigma \equiv V_t/\kappa_\sigma k_B T_0 \mathcal{A}$, we obtain explicit expressions for each element of the metric:

$$g_{LL} = N_t k_B T_0[\epsilon_\beta \tau_\beta (x^R)^2/(1-x^L)^3 + \epsilon_\alpha \tau_\alpha/(1-x^R) + 2/3 \times \epsilon_\beta^2 \tau_h/(1-x^L)^2], \tag{E5}$$

$$g_{LR} = g_{RL} = N_t k_B T_0\{\epsilon_\alpha \tau_\alpha x^L/(1-x^R)^2 + \epsilon_\beta \tau_\beta x^R/(1-x^L)^2 + 2/3 \times \epsilon_\alpha \epsilon_\beta \tau_h/[(1-x^L)(1-x^R)]\}, \tag{E6}$$

$$g_{RR} = N_t k_B T_0[\epsilon_\alpha \tau_\alpha (x^L)^2/(1-x^R)^3 + \epsilon_\beta \tau_\beta/(1-x^L) + 2/3 \times \epsilon_\alpha^2 \tau_h/(1-x^R)^2]. \tag{E7}$$

To obtain the optimal symmetry-breaking protocols, we need to numerically evaluate the geodesic paths connecting $(0,0)$ and $(\epsilon_\alpha, \epsilon_\beta)$ by solving the geodesic equation (9). For ideal gases, the Christoffel symbols are analytically obtained as

$$\frac{\Gamma_{LLL}}{N_t k_B T_0} = \frac{2\epsilon_\beta^2 \tau_h}{3(1-x^L)^3} + \frac{3\epsilon_\beta \tau_\beta (x^R)^2}{2(1-x^L)^4}, \tag{E8}$$

$$\frac{\Gamma_{RRR}}{N_t k_B T_0} = \frac{2\epsilon_\alpha^2 \tau_h}{3(1-x^R)^3} + \frac{3\epsilon_\alpha \tau_\alpha (x^L)^2}{2(1-x^R)^4}, \tag{E9}$$

$$\frac{\Gamma_{LRL}}{N_t k_B T_0} = \frac{\epsilon_\beta \tau_\beta}{2(1-x^L)^2} + \frac{\epsilon_\alpha \tau_\alpha x^L}{(1-x^R)^3}, \tag{E10}$$

$$\frac{\Gamma_{LRR}}{N_t k_B T_0} = \frac{\epsilon_\alpha \tau_\alpha}{2(1-x^R)^2} + \frac{\epsilon_\beta \tau_\beta x^R}{(1-x^L)^3}, \tag{E11}$$

$$\frac{\Gamma_{RRL}}{N_t k_B T_0} = \frac{\epsilon_\beta \tau_\beta}{2(1-x^L)^2} + \frac{\epsilon_\alpha \tau_\alpha x^L}{(1-x^R)^3} + \frac{2\epsilon_\alpha \epsilon_\beta \tau_h/3}{(1-x^L)(1-x^R)^2}, \tag{E12}$$

$$\frac{\Gamma_{LLR}}{N_t k_B T_0} = \frac{\epsilon_\alpha \tau_\beta}{2(1-x^R)^2} + \frac{\epsilon_\beta \tau_\beta x^R}{(1-x^L)^3} + \frac{2\epsilon_\alpha \epsilon_\beta \tau_h/3}{(1-x^R)(1-x^L)^2}. \tag{E13}$$

The Christoffel symbols Γ^i_{jk} in the geodesic equations are obtained via $\Gamma^i_{jk} \equiv g^{il}\Gamma_{ljk}$ with the inverse metric g^{ij}.

APPENDIX F: SINGULARITIES OF GEODESIC EQUATIONS AND EVOLUTION EQUATIONS

We analyze the singularities that arise when solving the geodesic equation (9) and the evolution equations (2) and (3).

Firstly, we observe that the metric tensor G at $(x^L, x^R) = (\epsilon_\alpha, \epsilon_\beta)$ is degenerate. For instance, for separating equally mixed ideal gases, it is explicitly given by

$$G = N_t k_B T_0 \left(\tau_\alpha + \tau_\beta + \frac{2}{3}\tau_h\right)\begin{pmatrix} 1 & 1 \\ 1 & 1 \end{pmatrix}, \tag{F1}$$

which induces the divergence of G^{-1}, and subsequently the divergence of Christoffel symbols Γ^k_{ij} at the target point $(\epsilon_\alpha, \epsilon_\beta)$. As a result, when searching for geodesic paths, we encounter a singularity near the target point, causing $dx^k/dt \to 0$. To achieve a numerical solution with given accuracy, we need to decrease the step length of solving to match the decrease of the derivative of x^k. This causes the step length to approach 0, and consequently causes the divergence of required computational resources. Thus, the numerical solution should be terminated near the target point instead of when it is reached.

Secondly, given a control protocol $x^L(t)$ and $x^R(t)$, for the volumes, we numerically simulate the evolution using Eqs. (2) and (3). With a given operation time τ, the volumes are expressed explicitly as functions of time, i.e., $V_k(t) = V_t x^k(t)$. The evolution equations (2) and (3) have two removable singularities, at the beginning ($t = 0$) and at the end ($t = \tau$) of the separation process. Specifically, the particle densities in the left and right compartments, $c_{\alpha L} = N_{\alpha L}/V_L$ and $c_{\beta R} = N_{\beta R}/V_R$, take the form of $0/0$ at $t = 0$, and the particle densities in the middle compartment, $c_{\alpha M} = N_{\alpha M}/V_M$ and $c_{\beta M} = N_{\beta M}/V_M$, exhibit the same behavior at $t = \tau$. These singularities lead to computational difficulty when one is numerically simulating the evolution.

To overcome the computational difficulty posed by the aforementioned singularities, we choose the starting point and the target point to be slightly different from $(0,0)$ and $(0.5, 0.5)$. Specifically, we select the starting point as $(10^{-3}, 10^{-3})$ and the target point as $(0.5 - 10^{-3}, 0.5 - 10^{-3})$ for the separation of both ideal gases and van der Waals gases. By bypassing these two singularities, we can obtain the results without loss of accuracy.

[1] Arthur L. Kohl and R. Nielsen, *Gas Purification, Houston* (Gulf Pub., 1997).

[2] David S. Sholl and Ryan P. Lively, Seven chemical separations to change the world, Nature **532**, 435 (2016).

[3] F. G. Skinskey, Distillation control: For productivity and energy conservation, (1984).

[4] Andrew Mills, Richard H. Davies, and David Worsley, Water purification by semiconductor photocatalysis, Chem. Soc. Rev. **22**, 417 (1993).

[5] A. J. Hutt and S. C. Tan, Drug chirality and its clinical significance, Drugs **52**, 1 (1996).

[6] Robert L. Fahrner, Heather L. Knudsen, Carol D. Basey, Walter Galan, Dian Feuerhelm, Martin Vanderlaan, and Gregory S. Blank, Industrial purification of pharmaceutical antibodies: Development, operation, and validation of

chromatography processes, Biotechnol. Genet. Eng. Rev. **18**, 301 (2001).
[7] Bo Liu, Chong Ye, C. P. Sun, and Yong Li, Spatial enantioseparation of gaseous chiral molecules, Phys. Rev. A **104**, 013113 (2021).
[8] Neil M. Wade, Distillation plant development and cost update, Desalination **136**, 3 (2001).
[9] S. A. Avlonitis, K. Kouroumbas, and N. Vlachakis, Energy consumption and membrane replacement cost for seawater RO desalination plants, Desalination **157**, 151 (2003).
[10] W. J. Koros and G. K. Fleming, Membrane-based gas separation, J. Membr. Sci. **83**, 1 (1993).
[11] William J. Koros, Evolving beyond the thermal age of separation processes: Membranes can lead the way, AIChE J. **50**, 2326 (2004).
[12] A. K. Pabby, S. S. H. Rizvi, and A. M. S. Requena, *Handbook of Membrane Separations Chemical, Pharmaceutical, Food, and Biotechnological Applications, Second Edition* (Taylor and Francis Group, Florida, 2015), p. 878.
[13] T. A. Saleh and V. K. Gupta, *Nanomaterial and Polymer Membranes: Synthesis, Characterization, and Applications* (Elsevier Science & Technology Books, Amsterdam, 2016), p. 284.
[14] Christophe Castel and Eric Favre, Membrane separations and energy efficiency, J. Membr. Sci. **548**, 345 (2018).
[15] E. L. Cussler and Binay K. Dutta, On separation efficiency, AIChE J. **58**, 3825 (2012).
[16] William J. Koros and Ryan P. Lively, Water and beyond: Expanding the spectrum of large-scale energy efficient separation processes, AIChE J. **58**, 2624 (2012).
[17] Pedro J. J. Alvarez, Candace K. Chan, Menachem Elimelech, Naomi J. Halas, and Dino Villagrán, Emerging opportunities for nanotechnology to enhance water security, Nat. Nanotechnol. **13**, 634 (2018).
[18] Sadaf Noamani, Shirin Niroomand, Masoud Rastgar, and Mohtada Sadrzadeh, Carbon-based polymer nanocomposite membranes for oily wastewater treatment, Npj Clean Water **2**, 20 (2019).
[19] S. LI, SAPO-34 membranes for CO_2/CH_4 separation, J. Membr. Sci. **241**, 121 (2004).
[20] J. K. Adewole, A. L. Ahmad, S. Ismail, and C. P. Leo, Current challenges in membrane separation of CO2 from natural gas: A review, Int. J. Greenh. Gas Control. **17**, 46 (2013).
[21] Robert van Reis and Andrew Zydney, Bioprocess membrane technology, J. Membr. Sci. **297**, 16 (2007).
[22] Rui Xie, Liang-Yin Chu, and Jin-Gen Deng, Membranes and membrane processes for chiral resolution, Chem. Soc. Rev. **37**, 1243 (2008).
[23] O. FalkPedersen and H. Dannstrom, Separation of carbon dioxide from offshore gas turbine exhaust, Energy Convers. Manag. **38**, S81 (1997).
[24] Eric Favre, Carbon dioxide recovery from post-combustion processes: Can gas permeation membranes compete with absorption?, J. Membr. Sci. **294**, 50 (2007).
[25] Tim C. Merkel, Haiqing Lin, Xiaotong Wei, and Richard Baker, Power plant post-combustion carbon dioxide capture: An opportunity for membranes, J. Membr. Sci. **359**, 126 (2010).
[26] Na Zhang, Chenxu Wu, Juntian Zhang, Shuang Han, Yongzhen Peng, and Xiaoye Song, Impacts of lipids on the performance of anaerobic membrane bioreactors for food wastewater treatment, J. Membr. Sci. **666**, 121104 (2023).
[27] M. Mulder, in *Membrane Processes in Separation and Purification*, edited by J. Crespo and K. Böddeker (Springer Netherlands, Dordrecht, 1994), p. 445.
[28] M. G. Buonomenna and J. Bae, Membrane processes and renewable energies, Renewable Sustainable Energy Rev. **43**, 1343 (2015).
[29] V. Teplyakov, M. Shalygin, D. Syrtsova, and A. Netrusov, in *Current Trends and Future Developments on (Bio-) Membranes: Renewable Energy Integrated with Membrane Operations*, edited by Angelo Basile, Alfredo Cassano and Alberto Figoli (Elsevier, Amsterdam, 2019), p. 319.
[30] M. K. Purkait and R. Singh, *Membrane Technology in Separation Science* (Taylor and Francis Group, Boca Raton, 2018).
[31] Yonghong Wang, Lecheng Sheng, Xinru Zhang, Jinping Li, and Rong Wang, Hybrid carbon molecular sieve membranes having ordered Fe_3O_4@ZIF-8-derived microporous structure for gas separation, J. Membr. Sci. **666**, 121127 (2023).
[32] Yu Huang, Richard W. Baker, and Leland M. Vane, Low-energy distillation-membrane separation process, Ind. Eng. Chem. Res. **49**, 3760 (2010).
[33] Sato Yuki and Kansha Yasuki, Design of an energy-saving membrane separation module for algae cultivation, Chem. Eng. Trans. **88**, 781 (2021).
[34] A. Basile and A. Comite, *Current Trends and Future Developments on (Bio-)Membranes: Membrane Technology for Water and Wastewater Treatment – Advances and Emerging Processes* (Elsevier, Amsterdam, 2020).
[35] A. G. Fane, R. W. Schofield, and C. J. D. Fell, The efficient use of energy in membrane distillation, Desalination **64**, 231 (1987).
[36] H. B. Callen, *Thermodynamics and an Introduction to Thermostatistics*, 2nd ed. (Wiley, New York, 1985).
[37] K. Huang, *Statistical Mechanics*, 2nd ed. (Wiley, New York, 1987).
[38] F. L. Curzon and B. Ahlborn, Efficiency of a Carnot engine at maximum power output, Am. J. Phys. **43**, 22 (1975).
[39] Peter Salamon and Abrahan Nitzan, Finite time optimizations of a newton's law Carnot cycle, J. Chem. Phys. **74**, 3546 (1981).
[40] Anatoliy M. Tsirlin, Vladimir Kazakov, and Dmitrii V. Zubov, Finite-time thermodynamics: limiting possibilities of irreversible separation processes†, J. Phys. Chem. A **106**, 10926 (2002).
[41] F. Weinhold, Metric geometry of equilibrium thermodynamics, J. Chem. Phys. **63**, 2479 (1975).
[42] George Ruppeiner, Thermodynamics: A Riemannian geometric model, Phys. Rev. A **20**, 1608 (1979).
[43] Peter Salamon and R. Stephen Berry, Thermodynamic Length and Dissipated Availability, Phys. Rev. Lett. **51**, 1127 (1983).
[44] Gavin E. Crooks, Measuring Thermodynamic Length, Phys. Rev. Lett. **99**, 100602 (2007).
[45] David A. Sivak and Gavin E. Crooks, Thermodynamic Metrics and Optimal Paths, Phys. Rev. Lett. **108**, 190602 (2012).

[46] Matteo Scandi and Martí Perarnau-Llobet, Thermodynamic length in open quantum systems, Quantum **3**, 197 (2019).

[47] Jin-Fu Chen, C. P. Sun, and Hui Dong, Extrapolating the thermodynamic length with finite-time measurements, Phys. Rev. E **104**, 034117 (2021).

[48] Geng Li, Jin-Fu Chen, C. P. Sun, and Hui Dong, Geodesic Path for the Minimal Energy Cost in Shortcuts to Isothermality, Phys. Rev. Lett. **128**, 230603 (2022).

[49] Jin-Fu Chen, Optimizing Brownian heat engine with shortcut strategy, Phys. Rev. E **106**, 054108 (2022).

[50] Jianguo Xu and Rakesh Agrawal, Membrane separation process analysis and design strategies based on thermodynamic efficiency of permeation, Chem. Eng. Sci. **51**, 365 (1996).

[51] Stanislaw Sieniutycz and Anatoly Tsirlin, Finding limiting possibilities of thermodynamic systems by optimization, Phil. Trans. R. Soc. A **375**, 20160219 (2017).

[52] S. Sieniutycz and J. Jezowski, *"Optimization and qualitative aspects of separation systems"* in *Energy Optimization in Process Systems and Fuel Cells* (Elsevier, Amsterdam, 2018), Chap. 8, p. 273.

[53] B. Hille, *Ion Channels of Excitable Membranes* (Sinauer Associates, Sunderland, 2001).

[54] M. Berger, *A Panoramic View of Riemannian Geometry* (Springer-Verlag, Berlin, 2003).

[55] Yu-Han Ma, Ruo-Xun Zhai, Jinfu Chen, C. P. Sun, and Hui Dong, Experimental Test of the $1/\tau$-Scaling Entropy Generation in Finite-Time Thermodynamics, Phys. Rev. Lett. **125**, 210601 (2020).